Constraints on melt distribution from seismology: a case study in Ethiopia

J. O. S. HAMMOND[1]* & J.-M. KENDALL[2]

[1]*School of Earth and Planetary Sciences, Birkbeck, University of London, London WC1E 7HX, UK*

[2]*Department of Earth Sciences, University of Bristol, Bristol BS8 1RJ, UK*

**Corresponding author (e-mail: james.hammond@bbk.ac.uk)*

Abstract: Low seismic velocities and/or strong seismic anisotropy are often interpreted as being caused by partial melt. To better understand this, we used numerical modelling, varying the shape and amount of melt, to show how seismic phases are affected by melt. We observed that seismic waves are more sensitive to the shape than to the amount of melt. Rayleigh wave velocities were almost always reduced in the presence of melt, while Pn/wide-angle P-wave refraction and Love wave velocities showed low velocity anomalies for vertically aligned melt, but little anomaly for horizontally aligned melt. These data can therefore be used to determine the alignment of melt. Shear wave splitting/receiver functions showed strong anisotropy and can be used to constrain the strike of vertically aligned partial melt. We showed that melt in the mantle beneath Ethiopia is probably stored in low aspect ratio disc-like inclusions, suggesting that the melt is not in textural equilibrium. We estimated that 2–7% of the vertically aligned melt is stored beneath the Main Ethiopian Rift, >6% of the horizontally and vertically aligned melt is stored beneath the Red Sea Rift and 1–6% of the horizontally aligned melt is stored beneath the Danakil microplate. This supports the idea of strong shear-derived segregation of melt in the narrow Main Ethiopian Rift compared with that observed beneath Afar.

Volcanism at the Earth's surface is driven by the partial melting of rocks in the upper mantle and the buoyancy-driven ascent of melt to the surface. The presence of melt in the mantle can affect the strength of mantle rocks (Takei & Holtzman 2009) and thus affects mantle dynamics in tectonically active regions (Holtzman & Kendall 2010; Pommier *et al.* 2015). However, melt follows complex pathways to the surface (e.g. Kelemen *et al.* 1997; Holtzman & Kohlstedt 2007) and can pond at many depths before eruption (Annen *et al.* 2006). If we are to understand the processes that form the crust, drive tectonic plates and give rise to volcanoes, then we must understand the mechanisms by which melt is stored and transported.

In this study, we considered the sensitivity of a number of seismic phases (body waves and surface waves) commonly measured in volcanic settings to the presence of partial melt. This allowed us to determine the seismic attributes that are most sensitive to the presence of melt, thus guiding future studies about how to interpret seismic data. We applied this new understanding to unravelling the nature of melt distribution in the mantle beneath the Main Ethiopian and Red Sea rifts in Ethiopia.

Seismic images of melt

Laboratory experiments at high frequencies (>MHz) have shown that partial melt strongly affects seismic parameters (Faul *et al.* 1994) such as velocity and attenuation. More recent studies have suggested that these laboratory experiments can be extrapolated to field-scale seismic frequencies ($1–10^{-3}$ Hz) (Garapic *et al.* 2013). Relationships have been derived to extract melt fractions from seismic velocity anomalies (e.g. Hammond & Humphreys 2000) and, although these are often used to interpret melt volumes (West *et al.* 2001; Goes & van der Lee 2002; Stixrude & Lithgow-Bertelloni 2005; Stork *et al.* 2013), they are only valid for specific melt geometries and must be treated with caution. In addition, isotropic velocities are sensitive to variations in temperature (Jackson *et al.* 2002), composition (Karato & Jung 1998) and attenuation (Goes *et al.* 2012), all parameters that are expected to be anomalous in the presence of partial melt. Unravelling the nature of melt storage from isotropic velocities alone therefore remains difficult. Furthermore, seismic properties vary strongly with melt geometry (Kendall 1994; Hammond & Humphreys

From: WRIGHT, T. J., AYELE, A., FERGUSON, D. J., KIDANE, T. & VYE-BROWN, C. (eds) *Magmatic Rifting and Active Volcanism*. Geological Society, London, Special Publications, **420**, http://doi.org/10.1144/SP420.14

2000; Takei 2013), which further complicates the interpretation of isotropic velocity. Observations of seismic anisotropy have been used to characterize melt beneath volcanic settings where it shows particular sensitivity to the aspect ratio (the shape of the melt pockets/inclusions) and any preferential alignment of the melt (Kendall 1994; Hammond & Humphreys 2000; Bastow *et al.* 2010; Holtzman & Kendall 2010; Keir *et al.* 2011; Hammond 2014). Thus, although seismology clearly has the capability to image regions of melt in the crust and mantle, unravelling these signals requires careful analysis of both their isotropic and anisotropic signals.

Effects of melt on seismic velocities

To model the effects of melt on seismic properties, we calculated the elastic constants (using the Matlab toolbox MSAT; Walker & Wookey 2012) for aligned isolated melt pockets in a matrix material using effective medium modelling. We used the theory of Tandon & Weng (1984), which is based on the assumption that an applied stress is perturbed by inclusions, which, in general, can be either faster or slower than the surrounding medium. Tandon & Weng (1984) built on the formalism of Eshelby (1957), who determined the strain perturbation due to an ellipsoidal inclusion that may be either prolate or oblate in shape. Tandon & Weng (1984) generalized the theory to consider the effects of multiple aligned inclusions, together with the effects of the inclusion aspect ratio on the composite elastic moduli. A limitation of their theory is that, although the volume fraction of the inclusions can be very high, the inclusions cannot interact with each other. A more generalized theory can be used to model the effects of interconnected, low wetting angle inclusions (e.g. Chapman 2003), but this theory assumes penny-shaped inclusions and therefore cannot be used for higher wetting angle inclusions. Furthermore, frequency-dependent effects, which are sensitive to the size of the inclusion, are neglected and it is assumed that the melt inclusions are significantly smaller than the seismic wavelength (Al-Harrasi *et al.* 2011). Nevertheless, we were able to test a broad range of melt geometries using this theory to understand how different amounts and geometries of melt affect seismic waves.

The elastic constants were calculated using P- and S-wave velocities of 8.0 and 4.5 km s^{-1} and a density of 3.3 kg m^{-3} for the matrix material and 2.7 and 0.0 km s^{-1} and a density of 2.7 kg m^{-3} for the melt. We tested the effects of melt stored in isolated oblate spheroidal inclusions and tubules, analogous to melt stored along grain faces or grain boundaries, respectively (Schmeling 1985) (Fig. 1). In our models, we varied: (1) the amount of partial melt; (2) the aspect ratio (α) of the melt ($\alpha < 1$ for aligned discs, $\alpha = 1$ for spherical inclusions, $\alpha > 1$ for tubules); and (3) the direction of alignment (vertical or horizontal) of melt inclusions. The effective medium models produced elastic constants for each model (Fig. 1), from which it was possible to determine the velocity reduction and anisotropy that would be observed for a seismic phase travelling through a medium characterized by these elastic constants (Figs 2 & 3).

For typical melts in the upper mantle (e.g. silicate or carbonate melts), the dihedral angle is $<34^{\circ}$ (Minarik & Watson 1995; Holness 2005). At these low dihedral angles, melt is mobile and will wet grain boundaries (Garapic *et al.* 2013). As melt moves, it forms larger channels of melt through reactive transport, which increases the permeability further, allowing melt to move (Kelemen *et al.* 1997). A further mechanism to facilitate the ascent of melt is through the formation of melt-rich bands where the strain rates are high (e.g. Holtzman & Kohlstedt 2007). The modelling approach used here was analogous to any of these models of melt storage as long as the length scales of the melt structures were much smaller than the seismic wavelength. In this study, we only modelled vertically and horizontally aligned melts. This is valid as many melt transport and storage mechanisms are subhorizontal (e.g. sills, ponding at the base of the lithosphere) or subvertical (dykes, reactive transport). However, for more complex mechanisms (e.g. the shear-derived segregation of melt), the melt may be inclined (Holtzman & Kendall 2010). In these cases, we expect more complex relationships between the melt and seismic velocities/anisotropies than those explored here.

This simple modelling approach probably underestimates the effect of melt on seismic properties. For example, it does not account for the cuspate nature of the melt inclusions, which will cause stronger velocity reductions for each melt fraction (Hammond & Humphreys 2000). Also, this approach assumes that the inclusions are isolated and therefore no attenuation effects due to the interconnectivity of melt are considered. This can also act to increase the effect of melt on seismic velocities as a result of melt squirt flow, where the pressure gradients caused by the passage of the seismic wave cause fluid to flow along grain boundaries (Hammond & Humphreys 2000; Jakobsen & Chapman 2009; Garapic *et al.* 2013). As a result, the estimated melt fractions in this study are possibly too high, but this approach can help us to understand the relationships between melt and seismic velocity/anisotropy, yield useful estimates of the geometry of melt segregation and help us to understand the relative variations in melt segregation.

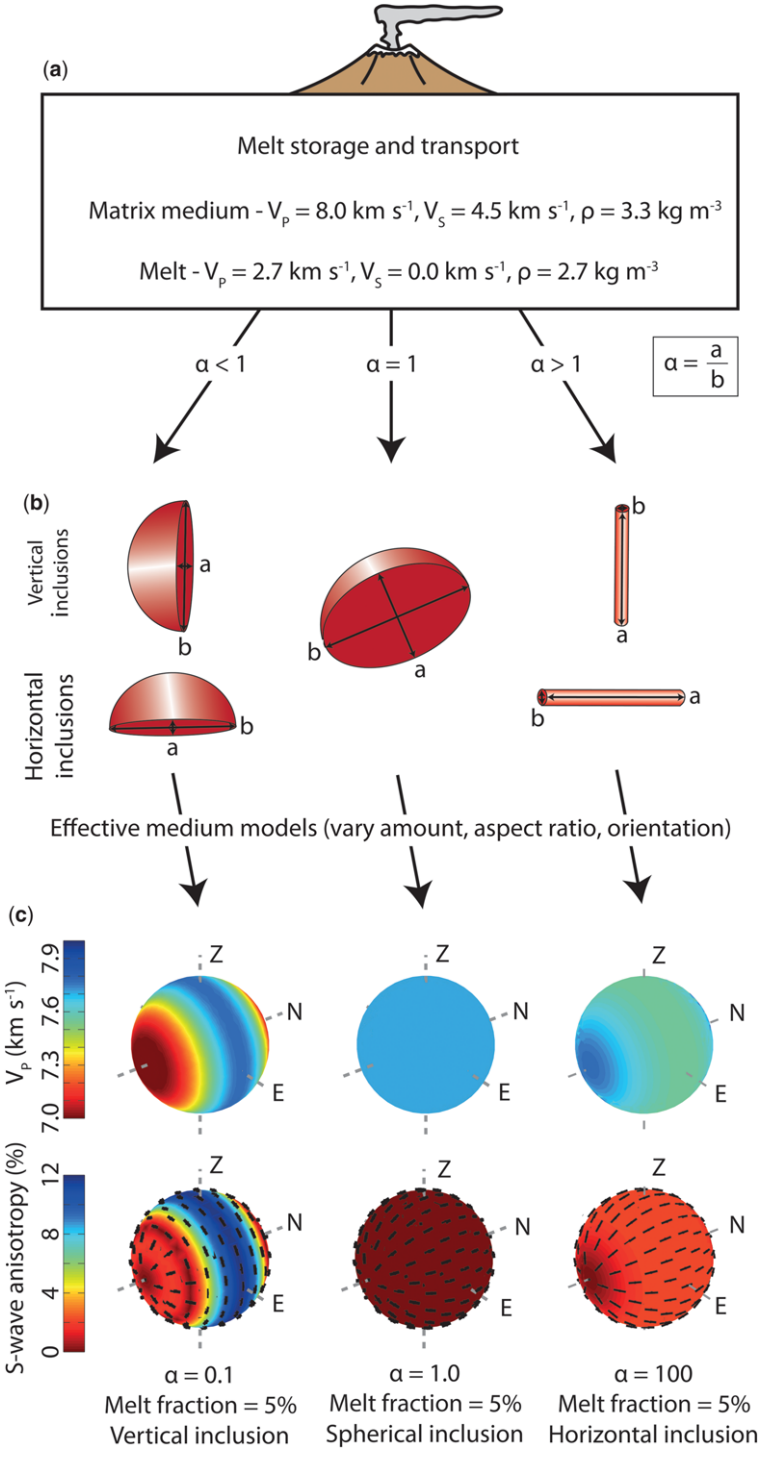

Fig. 1. Schematic diagram showing the effective medium modelling: (**a**) matrix and melt properties; (**b**) examples of melt geometries based on aspect ratios (α); and (**c**) results for three specific models with assumed parameters noted.

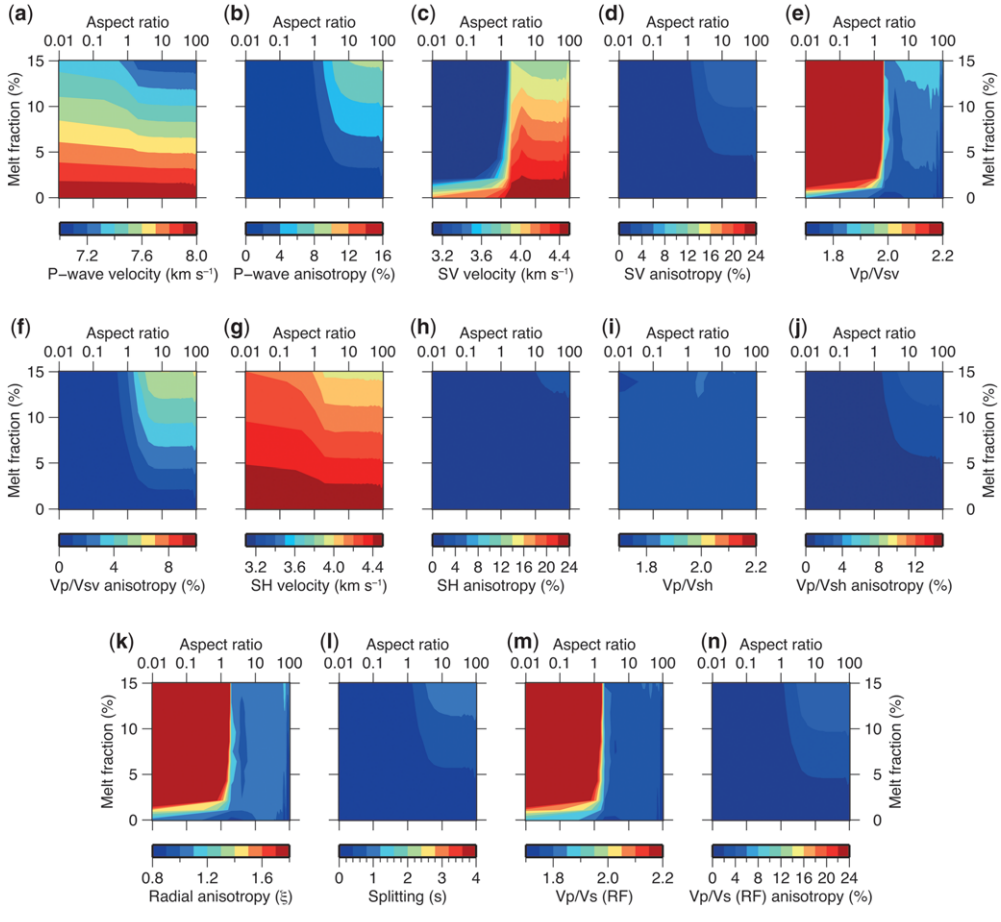

Fig. 2. Effect of horizontally aligned melt on different seismic waves. (**a**) Pn/refraction velocity (horizontally propagating P-wave (averaged from all back azimuths)); (**b**) Pn/refraction azimuthal anisotropy (azimuthal anisotropy in horizontally propagating P-wave); (**c**) Rayleigh wave velocity (horizontally propagating, vertically polarized shear wave (averaged from all back azimuths)); (**d**) Rayleigh wave azimuthal anisotropy (azimuthal anisotropy in horizontally propagating, vertically polarized shear wave); (**e**) Pn/refraction velocity/Rayleigh wave velocity (ratio of (a) and (c)); (**f**) Pn/refraction velocity/Rayleigh wave velocity azimuthal anisotropy (azimuthal anisotropy in ratio of (a) and (c)); (**g**) Love wave velocity (horizontally propagating, horizontally polarized shear wave (averaged from all back azimuths)); (**h**) Love wave velocity azimuthal anisotropy (azimuthal anisotropy in horizontally propagating, horizontally polarized shear wave); (**i**) Pn/refraction velocity/Love wave velocity (ratio of (a) and (g)); (**j**) Pn/refraction velocity/Love wave velocity azimuthal anisotropy (azimuthal anisotropy in ratio of (a) and (c)); (**k**) (Love wave velocity/Rayleigh wave velocity)^2 (square of ratio of (g) and (c)); (**l**) shear wave splitting (time difference between fast and slow shear waves in vertically propagating shear waves); (**m**) V_P/V_S from $H\kappa$ stacking from receiver functions (ratio of vertically travelling P-wave velocity and vertically propagating, dominant (fast or slow shear wave that has largest amplitude) vertically polarized shear wave (averaged from all back azimuths)); (**n**) azimuthal anisotropy in V_P/V_S from $H\kappa$ stacking from receiver functions (azimuthal anisotropy in (m)).

Figures 2 and 3 show the expected velocities and anisotropies for melt fractions from 0 to 15% and aspect ratios from 0.01 to 100 for horizontal and vertically aligned melts, respectively. We investigated the seismic phases that are commonly measured to understand mantle structure, such as horizontally travelling Pn, wide-angle refraction waves, surface waves (both Rayleigh and Love waves), and vertically travelling shear wave splitting and receiver functions.

Pn and wide-angle refraction data

Waves refracted at the Moho (Pn) are commonly used to infer seismic velocities in the uppermost mantle. They can be determined from impulsive,

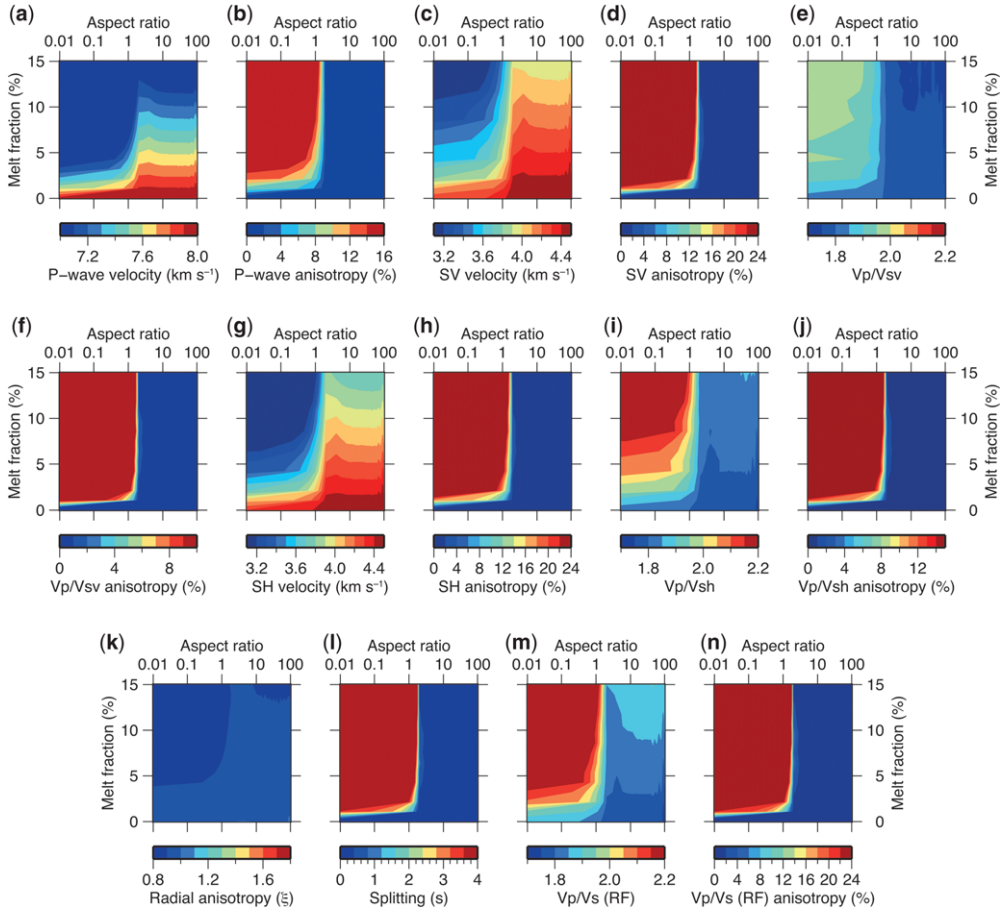

Fig. 3. Effect of vertically aligned melt on different seismic waves. (**a**) Pn/refraction velocity (horizontally propagating P-wave (averaged from all back azimuths)); (**b**) Pn/refraction azimuthal anisotropy (azimuthal anisotropy in horizontally propagating P-wave); (**c**) Rayleigh wave velocity (horizontally propagating, vertically polarized shear wave (averaged from all back azimuths)); (**d**) Rayleigh wave azimuthal anisotropy (azimuthal anisotropy in horizontally propagating, vertically polarized shear wave); (**e**) Pn/refraction velocity/Rayleigh wave velocity (ratio of (a) and (c)); (**f**) Pn/refraction velocity/Rayleigh wave velocity azimuthal anisotropy (azimuthal anisotropy in ratio of (a) and (c)); (**g**) Love wave velocity (horizontally propagating, horizontally polarized shear wave (averaged from all back azimuths)); (**h**) Love wave velocity azimuthal anisotropy (azimuthal anisotropy in horizontally propagating, horizontally polarized shear wave); (**i**) Pn/refraction velocity/Love wave velocity (ratio of (a) and (g)); (**j**) Pn/refraction velocity/Love wave velocity azimuthal anisotropy (azimuthal anisotropy in ratio of (a) and (c)); (**k**) (Love wave velocity/Rayleigh wave velocity)^2 (square of ratio of (g) and (c)); (**l**) shear wave splitting (time difference between fast and slow shear waves in vertically propagating shear waves); (**m**) V_P/V_S from $H\kappa$ stacking from receiver functions (ratio of vertically travelling P-wave velocity and vertically propagating, dominant (fast or slow shear wave that has largest amplitude) vertically polarized shear wave (averaged from all back azimuths)); (**n**) azimuthal anisotropy in V_P/V_S from $H\kappa$ stacking from receiver functions (azimuthal anisotropy in (m)).

artificial sources or measured from natural earthquakes. In active tectonic settings, the presence of low upper mantle P-wave velocities and azimuthal anisotropy have been used as evidence for the presence of melt (e.g. Ethiopia – Mackenzie *et al.* 2005; Maguire *et al.* 2006; Stork *et al.* 2013; Corbeau *et al.* 2014; Tibet – Hearn *et al.* 2004; Pei *et al.* 2007; the western USA – Hearn 1996; Buehler & Shearer 2014; and Turkey – Hearn & Ni 1994). Pn and wide-angle refracted waves spend the majority of their time propagating horizontally in the mantle, thus we investigated the effects of melt on horizontally propagating P-waves. As a comparison with Pn tomography studies, we took the average P-wave

velocity across all back-azimuths. The first observation was that the expected P-wave velocity was strongly dependent on the geometry of the melt. For horizontally aligned inclusions (Fig. 2a), low velocities occurred for large melt fractions stored with any inclusion shape, whereas for vertically oriented inclusions (Fig. 3a) the lowest velocities were seen for melt fractions in thin discs (low aspect ratios). Thus observations of low Pn velocity in the mantle suggest either high melt fractions or vertically aligned melt in disc-like inclusions. Interestingly, these models show that the absence of a Pn anomaly does not preclude the fact that melt is present. Significant amounts of melt can be stored as horizontally aligned low aspect ratio inclusions and give small (<0.2 km s^{-1}) reductions in P-wave velocity. A strong azimuthal anisotropy would be expected for aligned vertical discs or horizontally aligned tubular inclusions (Figs 2b & 3b), but this would not be observed for horizontally aligned low aspect ratio melt or vertically aligned high aspect ratio melt (Fig. 2b).

Surface wave data

The best estimates of upper mantle S-wave velocities come from surface wave studies. Many studies have highlighted low S-wave velocities in the crust and mantle as evidence for the presence of melt (e.g. Ethiopia – Sebai *et al.* 2006; Bastow *et al.* 2010; East Pacific Rise – Forsyth *et al.* 1998; Gulf of California – Wang *et al.* 2009). Typically, these studies use both Rayleigh waves (vertically polarized) and Love waves (horizontally polarized). As for the Pn velocities in the previous section, we averaged across all back-azimuths to estimate the average S-wave velocity. For Rayleigh waves, a strong velocity reduction was seen for both horizontally and vertically aligned melts (Figs 2c & 3c); however, the reduction was strongest for low aspect ratio horizontally aligned melts. For Love waves, a strong velocity reduction was only seen for vertically aligned low aspect ratio or horizontally aligned high aspect ratio melts. Little reduction was evident for horizontally aligned low aspect ratio or vertically aligned high aspect ratio melts (Figs 2g & 3g). For vertically aligned low aspect ratio melts, both Rayleigh (Fig. 3d) and Love waves (Fig. 3h) showed strong azimuthal anisotropy, but with stronger anisotropy for the Rayleigh waves. This difference in azimuthal anisotropy gave rise to a weak radial anisotropy for low aspect ratio vertically aligned melt (Fig. 3k). If data are available from only selected back-azimuths, then different azimuthal anisotropies for Love and Rayleigh waves could give rise to an apparent strong radial anisotropy. For example, a Rayleigh wave travelling sub-parallel to the strike of aligned low aspect ratio melt will propagate with a relatively fast seismic velocity, whereas a Love wave travelling the same path will propagate with a relatively slow velocity, giving rise to the apparent radial anisotropy. For horizontally aligned low aspect ratio melt, the radial anisotropy is strong with $V_{SH} > V_{SV}$, particularly at low aspect ratios (Fig. 2h), but no azimuthal anisotropy is expected (Fig. 2d, h).

A parameter that can be used to distinguish the geometry of melt is the ratio of Pn velocity to surface wave velocity. For horizontally aligned melt, a large V_P/V_{SV} would be expected for moderate amounts of melt with aspect ratios <1 (Fig. 2e). However, if melt is aligned vertically, on average little anomaly in V_P/V_{SV} is observed (Fig. 3e), although V_P/V_{SV} exhibits a strong azimuthal anisotropy (Fig. 2f). Conversely, for horizontal low aspect ratio melts little anomaly was expected for V_P/V_{SH} (Fig. 2i), but an increase in V_P/V_{SH} was observed for vertically aligned low aspect ratio melts (Fig. 3i).

Shear wave splitting

Shear wave splitting in subvertically propagating body waves is one of the most common techniques used to estimate S-wave anisotropy in the crust and mantle. It has excellent lateral resolution and, with the use of earthquakes from many depth ranges (e.g. crustal earthquakes, teleseismic earthquakes), it can place depth constraints on the origin of the anisotropy. Shear wave splitting in horizontally travelling body waves is difficult to measure due to free surface and near-surface effects (Booth & Crampin 1985), so we only investigated the effect of melt on vertically propagating shear waves. The presence of aligned melt has been used to explain high shear wave splitting results (e.g. Ethiopia – Ayele *et al.* 2004; Kendall *et al.* 2005; Gao *et al.* 2010; Keir *et al.* 2011; Hammond *et al.* 2014; Japan – Wirth & Long 2010). Much like previous studies investigating the efficacy of melt to generate anisotropy (e.g. Blackman & Kendall 1997), we showed that vertically aligned melt with low aspect ratios can generate significant shear wave splitting for vertically travelling phases (e.g. SKS splitting) (Fig. 3l). Horizontally aligned low aspect ratio melt will produce very little anisotropy in vertically travelling phases (Fig. 2l). However, high aspect ratio horizontally aligned melt can produce small amounts of splitting for high melt fractions (Fig. 2l).

Receiver functions

P-wave to S-wave receiver functions are sensitive to the shear wave velocity in the crust and mantle. A common technique used to infer crustal structure is the $H-\kappa$ stacking technique that estimates crustal thickness and average V_P/V_S. Previous

studies have suggested that the presence of $V_P/V_S > 1.85$ provides evidence for significant melt in the crust (e.g. Ethiopia – Dugda *et al.* 2005; Stuart *et al.* 2006; Hammond *et al.* 2011; Tibet – Xu *et al.* 2007) and, more recently, Hammond (2014) showed that anisotropy in V_P/V_S can be explained by the presence of aligned melt. The presence of vertically oriented low aspect ratio melt (and, to a lesser degree, horizontally aligned high aspect ratio melt) will generate a split Ps phase as it enters the anisotropic medium. This gives rise to two values of V_P/V_S, one attributed to the fast S-wave and the other to the slow S-wave. The former will give rise to lower values of V_P/V_S, while the latter will be much higher. The relative amplitude of the split shear waves is controlled by the incoming back-azimuth, with back-azimuths close to the fast direction having a dominant fast shear wave and thus lower V_P/V_S than those events with a back-azimuth close to the slow axis. This manifests itself in a strong azimuthal anisotropy in V_P/V_S (Fig. 3n). No azimuthal anisotropy was seen for low aspect ratio horizontal inclusions or high aspect ratio vertical inclusions (Fig. 2n), but V_P/V_S can be elevated across all back-azimuths (Fig. 2m).

Summary

It is clear that the presence of melt, depending on the amount and geometry, can provide a wide range of seismic observations. If melt is stored in tubules or spherical inclusions, this does not reduce seismic velocities efficiently and produces minimal seismic anisotropy, meaning that higher melt fractions of a few per cent are required to explain most seismic anomalies. This suggests that, in the presence of observed strong anisotropy or reductions in velocity, melt is most likely to be stored in geometries more similar to aligned discs. It is easy to envisage scenarios where this may be the case, such as melt stored in dykes or sills, preferentially aligned shear bands in the mantle (Holtzman & Kendall 2010), or due to the melt wetting grain boundaries (Garapic *et al.* 2013). Conversely, this shows that the absence of a velocity anomaly does not mean that melt is not present, rather it may suggest that the melt network or storage characteristics are not efficient at producing a seismic anomaly.

To determine how different melt scenarios affect seismic data, we first placed some estimates on the errors in the different seismic datasets (based on estimates from studies beneath Ethiopia). For absolute velocities, we assumed that an anomaly >0.2 km s^{-1} would be observable above error (e.g. Bastow *et al.* 2010; Stork *et al.* 2013). For V_P/V_S estimated from receiver functions, an anomaly >0.05 km s^{-1} is required (e.g. Hammond 2014). An anisotropy of at least 2% is needed for us to consider it to be observable. This equates to *c.* 0.3 s of splitting for a 70 km thick layer (Hammond *et al.* 2014), but anisotropy is often a path-averaged effect, so lower amounts of anisotropy over a large region may be observable. Radial anisotropy was estimated using the approach of Sebai *et al.* (2006):

$$\xi = \left(\frac{V_{SH}}{V_{SV}}\right)^2, \quad (1)$$

where V_{SV} is the S_V velocity and V_{SH} is the S_H velocity. Using errors for absolute velocity of 0.2 km s^{-1} resulted in errors in ξ of *c.* 0.1. With these estimates of error, we constructed Table 1. This can be used as a guide to determine the range of plausible melt scenarios that can be detected using different seismic phases.

Seismically, one of the best indicators of melt is the Rayleigh wave velocity. This shows an observable velocity reduction for all scenarios except near-spherical/vertically aligned tubular inclusions with a low melt fraction (although these scenarios produce little observable anomaly in any dataset). At low melt fractions (<2%), Pn and Love waves are very sensitive to vertically aligned low aspect ratio melt, but show little anomaly in the presence of horizontally aligned low aspect ratio melt. This makes a combined analysis of Rayleigh and Love/Pn waves very useful in determining the likely geometry of the melt. Indeed, this has been observed beneath Toba, Sumatra, where Jaxybulatov *et al.* (2014) argued that low Rayleigh wave velocities and normal Love wave velocities showed that melt must be stored in sills in the lower crust beneath Toba volcano. One note of caution is that Rayleigh, Love and Pn wave velocities are typically determined for a path average, so may be limited in being able to distinguish smaller bodies of melt or spatial changes in melt storage. This example of strong radial anisotropy in the presence of horizontally aligned melt shows how measuring anisotropy is a powerful tool to determine melt storage characteristics. Vertically aligned low aspect ratio melt will give rise to strong azimuthal anisotropy, which would manifest in back-azimuthal variations in most seismic datasets and in shear wave splitting for vertically travelling shear waves and receiver functions. An example of this comes from the Main Ethiopian Rift (MER), where strong shear wave splitting together with azimuthal variations in Rayleigh and Love waves show that aligned melt is present in the mantle beneath the MER (Kendall *et al.* 2005; Bastow *et al.* 2010) and strong shear wave splitting together with azimuthal variations in V_P/V_S from receiver functions suggest aligned melt in the crust beneath Afar, Ethiopia (Keir *et al.* 2011; Hammond 2014). Horizontally aligned

Table 1. *Effects of melt on various seismic waves*

	Melt scenario	Pn	Pn anisotropy	SRW	SRW anisotropy	Pn/SRW	Pn/SRW anisotropy	SLW	SLW anisotropy	Pn/SLW	Pn/SLW anisotropy	Radial anisotropy ($\xi < 1$)	Radial anisotropy ($\xi > 1$)	S-wave splitting	V_P/V_S (RF)	V_P/V_S (RF) anisotropy
1	Horizontal inclusions Low melt fraction (<2%) Low aspect ratio (<0.1)	✗	✗	✓	✗	✓	✗	✗	✗	✗	✗	✗	✓	✗	✓	✗
2	Vertical inclusions Low melt fraction (<2%) Low aspect ratio (<0.1)	✓	✓	✓	✓	✓	✓	✓	✓	✓	✓	✗	✗	✓	✓	✓
3	Horizontal inclusions Low melt fraction (<2%) Moderate aspect ratio (0.1–0.5)	✗	✗	✓	✗	✓	✗	✗	✗	✗	✗	✗	✓	✗	✗	✗
4	Vertical inclusions Low melt fraction (<2%) Moderate aspect ratio (0.1–0.5)	✓	✓	✗	✓	✗	✓	✓	✓	✗	✗	✗	✗	✓	✗	✓
5	Spherical inclusions Low melt fraction (<2%) Aspect ratio = 1.0	✗	✗	✗	✗	✗	✗	✗	✗	✗	✗	✗	✗	✗	✗	✗
6	Horizontal inclusions Low melt fraction (<2%) High aspect ratio (1.5–100)	✗	✗	✗	✗	✗	✗	✗	✗	✗	✗	✗	✗	✗	✗	✗
7	Vertical inclusions Low melt fraction (<2%) High aspect ratio (1.5–100)	✗	✗	✗	✗	✗	✗	✗	✗	✗	✗	✗	✗	✗	✗	✗
8	Horizontal inclusions Moderate melt fraction (2–6%) Low aspect ratio (<0.1)	✓	✗	✓	✗	✓	✗	✗	✗	✗	✗	✗	✓	✗	✓	✗
9	Vertical inclusions Moderate melt fraction (2–6%) Low aspect ratio (<0.1)	✓	✓	✓	✓	✓	✓	✓	✓	✓	✓	✓	✗	✓	✓	✓
10	Horizontal inclusions Moderate melt fraction (2–6%) Moderate aspect ratio (0.1–0.5)	✓	✗	✓	✗	✓	✗	✗	✗	✗	✗	✗	✓	✗	✗	✗

11	Vertical inclusions Moderate melt fraction (2–6%) Moderate aspect ratio (0.1–0.5)	✓	✓	✓	✓	✗	✓	✓	✓	✗	✗	✗	✗	✓	✓	✓
12	Spherical inclusions Moderate melt fraction (2–6%) Aspect ratio = 1.0	✓	✗	✓	✗	✗	✗	✓	✗	✗	✗	✗	✗	✗	✗	✗
13	Horizontal inclusions Moderate melt fraction (2–6%) High aspect ratio (1.5–100)	✓	✓	✓	✓	✗	✓	✓	✗	✗	✗	✗	✗	✓	✗	✓
14	Vertical inclusions Moderate melt fraction (2–6%) High aspect ratio (1.5–100)	✓	✗	✓	✗	✗	✗	✓	✗	✗	✗	✗	✗	✗	✗	✗
15	Horizontal inclusions High melt fraction (>6%) Low aspect ratio (<0.1)	✓	✗	✓	✗	✓	✗	✓	✗	✗	✗	✗	✓	✗	✓	✗
16	Vertical inclusions High melt fraction (>6%) Low aspect ratio (<0.1)	✓	✓	✓	✓	✓	✓	✓	✓	✓	✓	✓	✗	✓	✓	✓
17	Horizontal inclusions High melt fraction (>6%) Moderate aspect ratio (0.1–0.5)	✓	✗	✓	✗	✓	✗	✓	✗	✗	✗	✗	✓	✗	✓	✗
18	Vertical inclusions High melt fraction (>6%) Moderate aspect ratio (0.1–0.5)	✓	✓	✓	✓	✗	✓	✓	✓	✓	✓	✓	✗	✓	✓	✓
19	Spherical inclusions High melt fraction (>6%) Aspect ratio = 1.0	✓	✗	✓	✗	✗	✗	✓	✗	✗	✗	✗	✗	✗	✗	✗
20	Horizontal inclusions High melt fraction (>6%) High aspect ratio (1.5–100)	✓	✓	✓	✓	✓	✓	✓	✓	✗	✓	✗	✗	✓	✗	✓
21	Vertical inclusions High melt fraction (>6%) High aspect ratio (1.5–2.0)	✓	✗	✓	✗	✗	✗	✓	✗	✓	✗	✓	✗	✗	✓	✗

A tick shows models where a seismic anomaly would probably be observed, whereas a cross shows those models where only a minimal anomaly would be observed.
RF, receiver function; SLW, surface Love wave; SRW, surface Rayleigh wave.

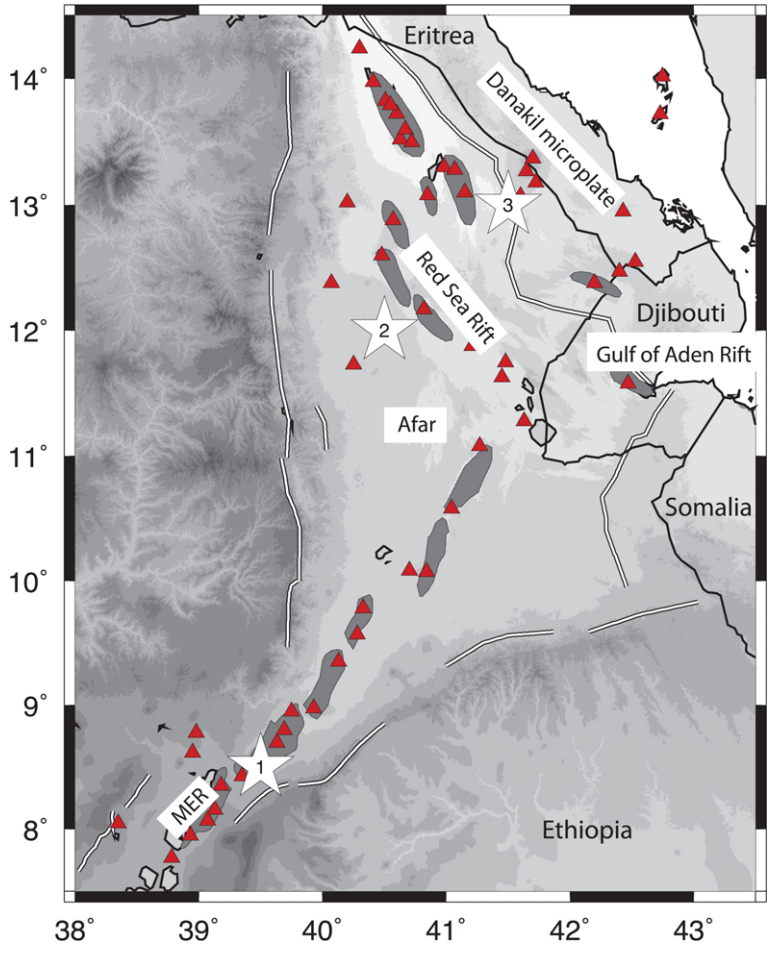

Fig. 4. Map showing the locations modelled in this study. (1) Main Ethiopian Rift (MER); (2) Afar (Dabbahu–Manda–Hararo) rift segment; (3) Afar (Danakil microplate). Solid triangles show Holocene volcanoes, white lines show major border faults and tectonic boundaries, and black lines show political boundaries.

high aspect ratio melt (tubes) will also result in some azimuthal anisotropy, but with lower magnitude. However, high melt fractions with tubular geometries can cause observable splitting or azimuthal anisotropy in surface waves and observable velocity reductions for Pn, Love and Rayleigh waves. In the presence of strong azimuthal anisotropy, care must be taken in interpreting absolute velocity variations. If a dataset is biased towards events from one azimuth, then this could lead to the inference of larger/smaller anomalies than may be expected for an average across all azimuths.

Melt in the mantle beneath Ethiopia

Ethiopia is host to the meeting of three tectonic rifts: the Red Sea, Gulf of Aden and Main Ethiopian rifts (Fig. 4). It is an ideal natural laboratory to study the final stages of continental break-up. Over the last two decades, many projects have focused on imaging the uppermost mantle to determine the driving processes of rifting beneath the region (Nyblade & Langston 2002; Maguire *et al.* 2003; Belachew *et al.* 2011; Hammond *et al.* 2011, 2013). These studies have led to much discussion about the role that melt plays in the rifting process, but what almost all the geophysical studies have shown is that melt must be present in the top few tens of kilometres throughout the crust and mantle beneath the MER (Gashawbeza *et al.* 2004; Bastow *et al.* 2005, 2008, 2010; Dugda *et al.* 2005; Keir *et al.* 2005; Kendall *et al.* 2005; Mackenzie *et al.* 2005; Benoit *et al.* 2006; Maguire *et al.* 2006; Stuart *et al.* 2006; Daly *et al.* 2008; Keranen *et al.* 2009;

Cornwell *et al.* 2010; Hammond *et al.* 2010) and Afar (Gao *et al.* 2010; Holtzman & Kendall 2010; Guidarelli *et al.* 2011; Hammond *et al.* 2011, 2013, 2014; Keir *et al.* 2011; Rychert *et al.* 2012; Desissa *et al.* 2013; Stork *et al.* 2013; Hammond 2014; Armitage *et al.* 2015), suggesting that the injection of magma into the lithosphere plays a key role in accommodating the strain associated with tectonic break-up (Kendall *et al.* 2005).

However, to date, our understanding of the details of melt segregation has remained unclear. For example, estimates from Pn tomography suggest that *c.* 3% melt is present at uppermost mantle depths beneath the Dabbahu–Manda–Hararo (DMH) rift segment in Afar (Stork *et al.* 2013); however, magnetotelluric studies suggest upwards of 12% melt is present (Desissa *et al.* 2013). Pommier & Garnero (2014) suggested that the composition of the melt could partly explain this discrepancy because peridotitic melts are more conductive than basaltic melts, meaning that lower melt fractions (3–13%) could explain the magnetotelluric data. There is much evidence from measurements of anisotropy to suggest that melt is aligned beneath Ethiopia (Kendall *et al.* 2005; Sebai *et al.* 2006; Sicilia *et al.* 2008; Bastow *et al.* 2010; Hammond *et al.* 2010, 2014; Keir *et al.* 2011; Hammond 2014). As shown here and discussed previously (Kendall 1994; Hammond & Humphreys 2000), this alignment, together with the shape of the melt, can change the sensitivity of seismic waves to melt. For example, 1% melt stored at low aspect ratios could, in fact, give a larger seismic anomaly than 10% melt in spherical or tubule-shaped inclusions (Figs 2 & 3). This raises the question: what range of models of melt can explain the observed seismic anomalies?

In this study, we focused on the nature of melt storage in the uppermost mantle. Estimates of the depth of melt initiation vary from 75 to 90 km beneath the MER and Afar (Rooney *et al.* 2005; Hammond *et al.* 2010; Rychert *et al.* 2012; Ferguson *et al.* 2013; Armitage *et al.* 2015). The crustal thickness varies from <35 km below the MER (Mackenzie *et al.* 2005; Maguire *et al.* 2006) to <26 km beneath Afar (Makris & Ginzburg 1987; Dugda *et al.* 2005; Hammond *et al.* 2011). As a result, we looked for estimates of seismic velocity and anisotropy at *c.* 50 km depth as representative of melt in the mantle beneath the MER and Afar. We choose three areas that have been suggested to be underlain by melt, but which are related to different stages in the rifting process: (1) the MER – an area of late-stage continental break-up; (2) the DMH rift segment in Afar – an area where incipient ocean spreading is thought to occur; and (3) the Danakil microplate (DM) in Afar – a suspected microplate located between the current location of rifting in Afar and the Red Sea between Eritrea and Yemen (Fig. 4).

Table 2 shows the constraints used for the various regions. The P-wave velocities are from wide-angle refraction studies in the MER (Mackenzie *et al.* 2005; Maguire *et al.* 2006) and a Pn tomography study in Afar (Stork *et al.* 2013). The S-wave velocities are from the surface wave model of Fishwick (2010). This study inverted Rayleigh waves, so these estimates are for the S_V velocities. Estimates of shear wave splitting are from Hammond *et al.* (2014). This study used multi-layer inversions to identify an upper layer of anisotropy, probably related to melt in the uppermost mantle underlain by anisotropy due to flow in the mantle. We used the upper layer estimates of anisotropy only. To obtain estimates of anisotropy in the mantle, we removed the 0.1–0.4 s of splitting estimated for the crust from the receiver function studies

Table 2. *Estimates of seismic velocity and anisotropy beneath Ethiopia*

	Afar (Dabbahu–Manda–Hararo rift fragment) 12° N, 40.5° E	References	Afar (Danakil microplate), 13° N, 41.5° E	References	Main Ethiopian Rift, 8.5° N, 39.5° E	References
P-wave velocity (km s^{-1})	7.2 ± 0.3	Stork *et al.* (2013)	8.1 ± 0.4	Stork *et al.* (2013)	7.5 ± 0.2	Maguire *et al.* (2006)
S-wave velocity (km s^{-1})	3.8 ± 0.2	Fishwick (2010)	3.9 ± 0.2	Fishwick (2010)	4.2 ± 0.2	Fishwick (2010)
S-wave splitting (s)	0.3–1.3	Hammond *et al.* (2014), Hammond (2014)	<0.3	Hammond *et al.* (2014), Hammond (2014)	1.1–1.6	Hammond *et al.*, (2014), Hammond (2014)
Radial anisotropy (ξ)	1.0–1.2	Sebai *et al.* (2006)	1.0–1.2	Sebai *et al.* (2006)	0.6–1.0	Bastow *et al.* (2010)

beneath the DMH rift segment, Afar (Hammond 2014) and assumed that a similar amount existed in the crust beneath the MER, a reasonable assumption given the high splitting for upper crustal earthquakes (Keir *et al.* 2005). Finally, we used estimates of radial anisotropy (equation 1) from the regional surface wave study of Sebai *et al.* (2006) in Afar and the detailed local study of the MER of Bastow *et al.* (2010). The Sebai *et al.* (2006) study was at low resolution (*c.* 500 km lateral resolution), so care must be taken in using these constraints to infer lateral variations between the three locations presented here. For the Bastow *et al.* (2010) constraint for the MER, the best-resolved ray paths were rift-parallel and the inferred orientation of melt pockets was obtained from shear wave splitting and surface waves (Kendall *et al.* 2005; Bastow *et al.* 2010).

In comparing different parts of the rift system, we assumed that the properties of the mantle were unchanged. In reality, thermal structure, geodynamic flow, lithospheric topography and the composition of the mantle will all affect the rock matrix properties, the depth of melt initiation and the amount of melting. Also, realistic melting models show that the style of melting will vary from its initiation at depth to storage at shallower depths. Despite this, this simple modelling exercise can place some first-order constraints on the distribution of melt beneath Ethiopia.

A first assessment can be made qualitatively using Table 1. Extremely low P-wave and Rayleigh wave velocities were observed beneath the DMH rift segment, together with high shear wave splitting and a suggestion of $\xi > 1$ ($V_{SH} > V_{SV}$) (although estimates of ξ are poorly constrained). Ignoring the estimates of ξ, melt scenarios 2, 9, 11, 13, 16, 18 and 20 fitted these data, suggesting moderate to high melt fractions with predominantly vertically aligned low aspect ratio melts or a very high melt fraction with a horizontally aligned high aspect ratio melt. Only a small Pn anomaly was observed beneath the DM. However, a strong V_{SV} anomaly was present. Little shear wave splitting was observed and there was a suggestion of $\xi > 1$. Again, ignoring ξ, melt scenarios 1 and 3 fit these data, suggesting low melt fractions preferentially aligned horizontally. Finally, beneath the MER, strong P- and SV-wave anomalies were present, with strong splitting and $\xi < 1$ for rift-parallel paths. Melt scenarios 9, 16 and 18 fit these data, suggesting vertically aligned moderate to high melt fractions with low/moderate aspect ratios.

These results make sense intuitively, with strong vertical alignments of melt beneath the narrow MER and Afar rifts, as suggested by studies using individual datasets (Kendall *et al.* 2005; Bastow *et al.* 2010; Hammond *et al.* 2010, 2014), although Hammond *et al.* (2014) suggested that the low degree of splitting away from the rift in Afar showed that horizontal melts were probably present. The next step was to see whether it was possible to perform a more quantitative approach and place better constraints on the range of melt models that can fit these data.

Melt segregation inversions

To invert the data, we used the same approach as outlined in the modelling section. However, we constrained our models using the observations summarized in Table 2. We varied the melt fraction (0–15%) and the aspect ratio (0.01–100) of vertical and horizontal inclusions and used a Voight–Ruess–Hill average to generate a composite medium. We also tested cases where only horizontal or vertical inclusions were present. This is similar to the approach used to invert receiver function estimates of V_P/V_S for melt geometries in the crust beneath Afar, Ethiopia (Hammond 2014). An important consideration is that we ignored any effects from preferred lattice orientations or other shape-preferred orientations from fine-scale layering and also any thermal or compositional effects, thus we may have overestimated the effects of melt-related anisotropy and an overall reduction in velocity.

We estimated P-wave and S-wave velocities for horizontally travelling waves (equivalent to Pn, refraction and surface wave studies) by averaging the velocities across all back-azimuths (an approach similar to surface wave and Pn inversions). For the S-wave velocity we used the vertically polarized wave for comparisons with Rayleigh wave inversions and horizontally polarized waves for comparisons with Love waves. We estimated the amount of shear wave splitting for a vertically propagating wave through a layer 70 km (DMH and DM) or 60 km (MER) thick. This is based on a likely depth of initial melting of <90 km (Rooney *et al.* 2005; Hammond *et al.* 2010; Rychert *et al.* 2012; Ferguson *et al.* 2013; Armitage *et al.* 2015) and a crust 20 km (Afar; Hammond *et al.* 2011) and 30 km (MER; Maguire *et al.* 2006) thick. Finally, radial anisotropy was estimated using equation (1).

For Afar, we estimated the average V_{SV} and V_{SH} across all back-azimuths before calculating ξ. This is because Sebai *et al.* (2006) based their estimates on V_{SV} and V_{SH} inversions from all back-azimuths. However, as this model lacks detailed resolution, we also tested the Afar results without the Sebai *et al.* (2006) constraint. For the MER we estimated ξ using melt-parallel ray paths only, similar to the ray path coverage of (Bastow *et al.* 2010) (assuming melt is aligned in the orientation of the rift; Kendall *et al.* 2005).

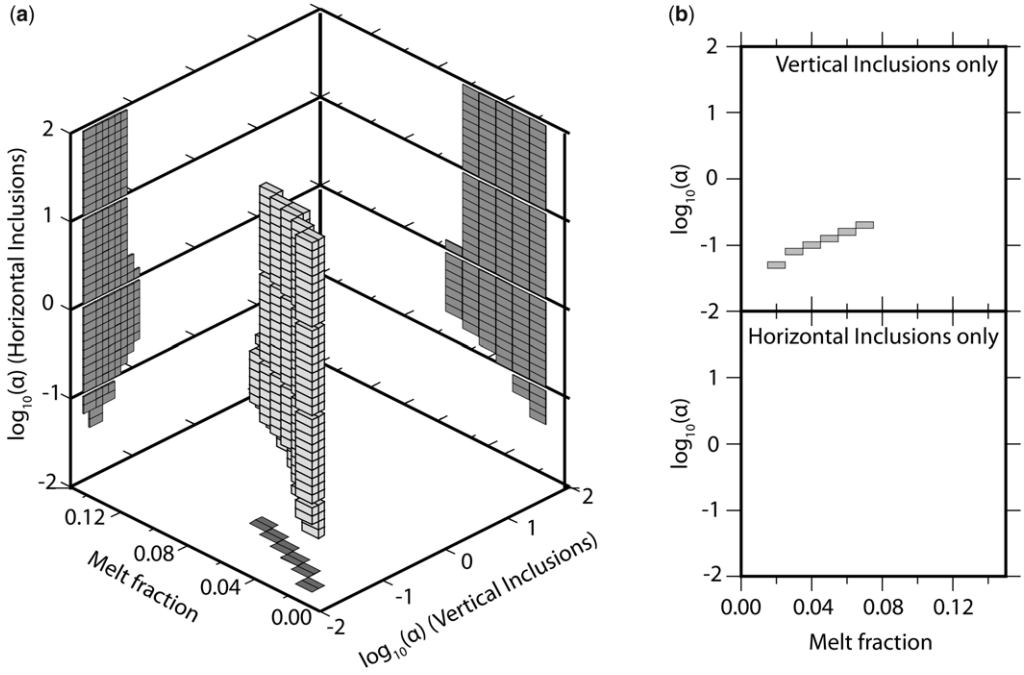

Fig. 5. Inversion for melt fraction, aspect ratio and geometry for the Main Ethiopian Rift: (**a**) inversions for a mixture of horizontal and vertically aligned melt; (**b**) inversions for vertical (top) and horizontal (bottom) aligned melt only. The light grey region shows all models that fit the seismic constraints. The dark grey region is a projection of the models that fit the seismic constraints.

MER

A number of observations were made beneath the MER (Fig. 5, Table 3).

(1) Low aspect ratio (0.02–0.2) vertically oriented melt must be present.
(2) Melt solely stored in spheres or tubules cannot explain the data.
(3) If only vertically aligned melt is present, then it must have an aspect ratio <0.2 (for 7% melt) and <0.05 (for 2% melt).
(4) Horizontally aligned melt is not required, but if it is present, then melt fractions are between 2 and 7% and the vertically aligned melt has aspect ratios between 0.02 and 0.10. There is no constraint on the aspect ratios of any horizontally aligned melt.

Table 3. *Range of models that can explain seismic observations beneath the Main Ethiopian Rift*

Main Ethiopian Rift (8.5° N, 39.5° E)	Melt fraction	Aspect ratio (vertical)	Aspect ratio (horizontal)
Disc-shaped vertical inclusions and any shaped horizontal inclusions	0.02–0.07	0.02–0.1	0.04–100
Tubular-shaped vertical inclusions and any shaped horizontal inclusions			
Disc-shaped horizontal inclusions and any shaped vertical inclusions	0.02–0.07	0.02–0.1	0.04–1
Tubular-shaped horizontal inclusions and any shaped vertical inclusions	0.02–0.07	0.02–0.1	1–100
Disc-shaped vertical inclusions and disc-shaped horizontal inclusions	0.02–0.07	0.02–0.1	0.04–1
Tubular-shaped vertical inclusions and tubular-shaped horizontal inclusions			
Vertical inclusions only (any aspect ratio)	0.02–0.07	0.05–0.2	–
Horizontal inclusions only (any aspect ratio)			

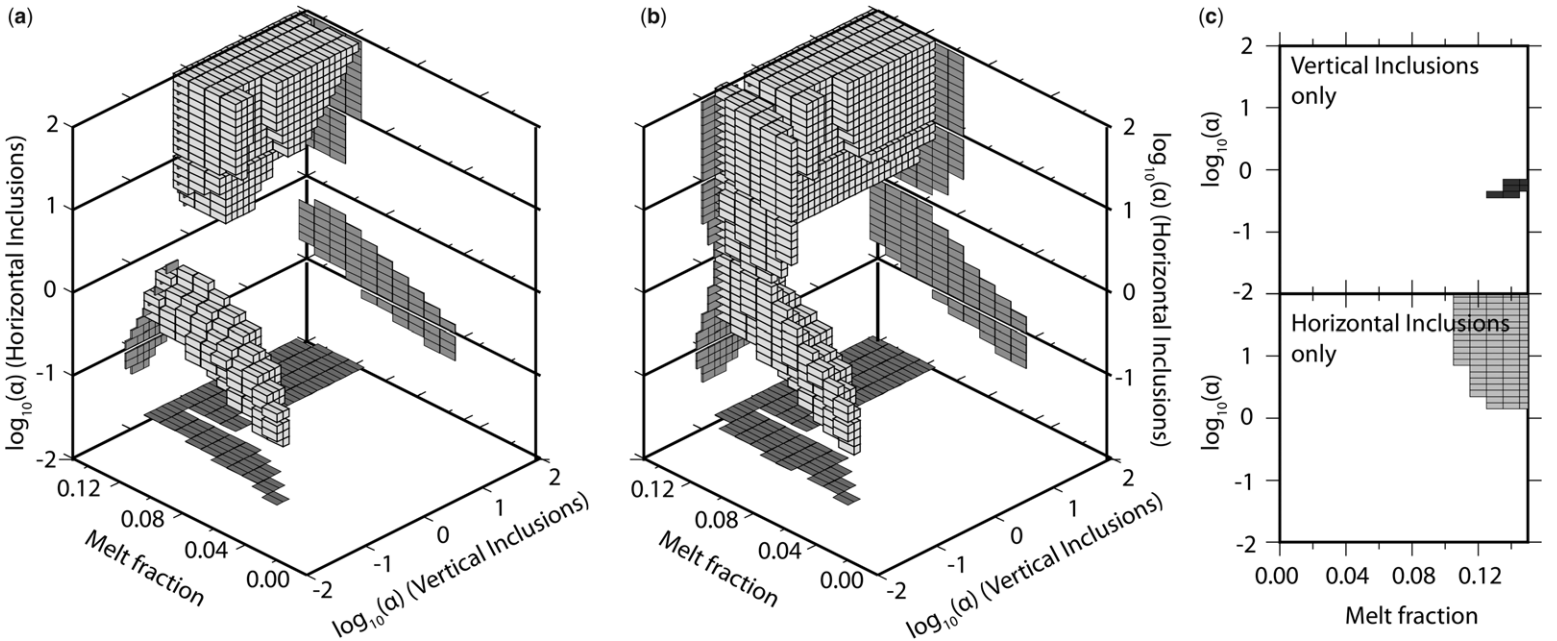

Fig. 6. Inversion for melt fraction, aspect ratio and geometry for Afar (Dabbahu–Manda–Hararo rift fragment). (a, b) Inversion results for a mixture of horizontal and vertically aligned melt (only horizontal and vertical inclusions were tested) (**a**) includes constraints on radial anisotropy from Sebai *et al.* (2006); (**b**) excludes constraints on radial anisotropy; (**c**) inversions for vertical (top) and horizontal (bottom) aligned melt only. (a, b) Light grey region shows all the models that fit the seismic constraints. Dark grey region is a projection of the models that fit the seismic constraints. (c) Light grey region includes constraints on radial anisotropy from Sebai *et al.* (2006), dark grey regions exclude constraints on radial anisotropy.

Table 4. *Range of models that can explain seismic observations beneath Afar (Dabbahu–Manda–Hararo rift fragment)*

Afar (Dabbahu–Manda–Hararo rift fragment) (12° N, 40.5° E)	Melt fraction	Aspect ratio (vertical)	Aspect ratio (horizontal)
Disc-shaped vertical inclusions and any shaped horizontal inclusions	0.06–0.15	0.1–1	0.05–100
Tubular-shaped vertical inclusions and any shaped horizontal inclusions	0.12–0.15	1–100	3–100
Disc-shaped horizontal inclusions and any shaped vertical inclusions	0.06–0.15	0.1–0.6	0.05–0.5
Tubular-shaped horizontal inclusions and any shaped vertical inclusions	0.12–0.15	0.8–100	3–100
Disc-shaped vertical inclusions and disc-shaped horizontal inclusions	0.06–0.15	0.1–0.6	0.05–0.5
Tubular-shaped vertical inclusions and tubular-shaped horizontal inclusions	0.12–0.15	1–100	3–100
Vertical inclusions only (any aspect ratio)			
Horizontal inclusions only (any aspect ratio)	0.11–0.15		2–100

Afar: DMH rift segment

Beneath the DMH rift segment, a number of observations were made (Fig. 6, Table 4).

(1) Both low aspect ratio and high aspect ratio melts can explain the seismic observations.
(2) If melt is stored in discs ($\alpha < 1$), then melt fractions are >6%; both horizontal and vertical melt must be present.
(3) If melt is stored in tubes ($\alpha > 1$), then melt fractions are >11%. Horizontal high aspect ratio melts alone can explain the seismic observations.
(4) If melt fraction = 6%, then vertical melt has aspect ratios of 0.1–0.13 and horizontal melt has aspect ratios between 0.05 and 0.1.
(5) If melt fraction = 15%, then vertical melt has aspect ratios between 0.25 and 100 and horizontal melt has aspect ratios between 0.16 and 0.40 or 3 and 100.

The results do not change considerably if the radial anisotropy constraints are not included in the inversion. The main difference is that we cannot rule out the possibility that more higher aspect ratio melts at high melt fractions may be present (Fig. 6, Table 5).

Afar: DM

Beneath DM three observations were made (Fig. 7, Table 6).

(1) Horizontally aligned melt must be present.
(2) If only horizontally aligned melt is present, then it has aspect ratios between 0.13 (4% melt) and 0.2 (6% melt).
(3) Vertically aligned melt is not required, but if it is present then melt fractions are constrained between 1 and 5% and horizontal inclusions have aspect ratios <0.1 and vertical inclusions have aspect ratios >0.08.

Again, removing the radial anisotropy constraint does not change these observations. It allows models of horizontal melt with lower aspect ratios and lower melt fractions to fit the data (Fig. 7, Table 7).

Table 5. *Range of models that can explain seismic observations beneath the Afar (Dabbahu–Manda–Hararo), but not including constraints on radial anisotropy*

Afar (Dabbahu–Manda–Hararo) (12° N, 40.5° E)	Melt fraction	Aspect ratio (vertical)	Aspect ratio (horizontal)
Disc-shaped vertical inclusions and any shaped horizontal inclusions	0.06–0.15	0.1–1	0.04–100
Tubular-shaped vertical inclusions and any shaped horizontal inclusions	0.12–0.15	1–100	3–100
Disc-shaped horizontal inclusions and any shaped vertical inclusions	0.06–0.15	0.1–0.63	0.04–1
Tubular-shaped horizontal inclusions and any shaped vertical inclusions	0.10–0.15	0.13–100	1–100
Disc-shaped vertical inclusions and disc-shaped horizontal inclusions	0.06–0.15	0.1–0.63	0.04–1
Tubular-shaped vertical inclusions and tubular-shaped horizontal inclusions	0.12–0.15	1–100	3–100
Vertical inclusions only (any aspect ratio)	0.13–0.15	0.4–0.63	
Horizontal inclusions only (any aspect ratio)	0.11–0.15		2–100

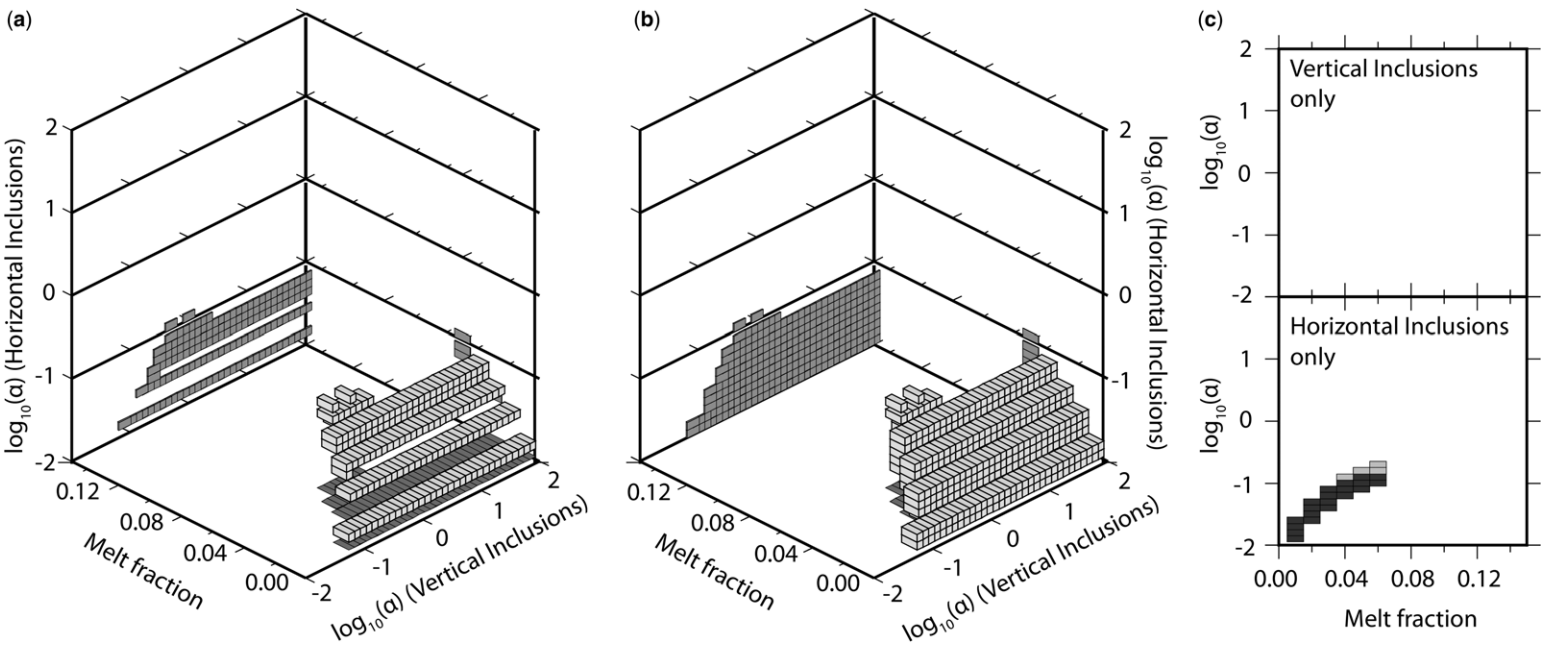

Fig. 7. Inversion for melt fraction, aspect ratio and geometry for Afar (Danakil microplate). (a, b) Inversion results for a mixture of horizontal and vertically aligned melt: (**a**) includes constraints on radial anisotropy from Sebai *et al.* (2006); (**b**) excludes constraints on radial anisotropy; (**c**) shows inversions for vertical (top) and horizontal (bottom) inclusions only. (a, b) Light grey region shows all models that fit the seismic constraints. Dark grey region is a projection of the models that fit the seismic constraints. (c) Light grey region includes constraints on radial anisotropy from Sebai *et al.* (2006), dark grey regions exclude constraints on radial anisotropy.

Table 6. *Range of models that can explain seismic observations beneath Afar (Danakil microplate)*

Afar (Danakil microplate) (13° N, 41.5° E)	Melt fraction	Aspect ratio (vertical)	Aspect ratio (horizontal)
Disc-shaped vertical inclusions and any shaped horizontal inclusions	0.01–0.05	0.08–1	0.013–0.1
Tubular-shaped vertical inclusions and any shaped horizontal inclusions	0.01–0.05	1–100	0.013–0.1
Disc-shaped horizontal inclusions and any shaped vertical inclusions	0.01–0.05	0.08–100	0.013–0.1
Tubular-shaped horizontal inclusions and any shaped vertical inclusions			
Disc-shaped vertical inclusions and disc-shaped horizontal inclusions	0.01–0.05	0.08–1	0.013–0.1
Tubular-shaped vertical inclusions and tubular-shaped horizontal inclusions			
Vertical inclusions only (any aspect ratio)			
Horizontal inclusions only (any aspect ratio)	0.04–0.06		0.13–0.2

Discussion

To a first order, the inversion results support the qualitative assessment discussed earlier. Moderate to large amounts of melt, predominantly aligned vertically, are found beneath the MER and DMH, but away from the rift beneath the DM the melt is predominantly aligned horizontally and can be explained by relatively small amounts of melt. This supports previous observations in both the MER (Kendall *et al.* 2005; Bastow *et al.* 2010; Hammond *et al.* 2010, 2014) and Afar (Hammond *et al.* 2014). However, with this study we can now place some constraints on the likely shapes and amounts of melt in these regions. The MER must have significant vertically aligned melt with an aspect ratio <0.2. Melt beneath the Red Sea Rift in Afar requires more melt ($>6\%$) than the MER (2–7%), with a mixture of horizontal and vertically aligned melt. The mantle beneath the DM does not need particularly large amounts of melt (1–5%), but this must be stored in low aspect ratio horizontally aligned structures ($\alpha < 0.2$).

Melt present in the mantle (at fractions less than a few per cent) under isotropic stress conditions would be expected to reach textural equilibrium (Takei 2013). This would probably form a homogeneous network of interconnected tubules (Takei 2013). Our inversions show that this is probably not the case beneath the MER and much of Afar. Melt stored in low aspect ratio disc-like inclusions fits the data better than spheres or tubes (Tables 3–7). This means that if melt is stored at the grain scale, it is probably wetting the grain boundaries rather than the grain edges, similar to that seen in laboratory experiments (Garapic *et al.* 2013). Laboratory experiments on rocks show that, in the presence of uniaxial compression and shear, melt aligns on the grain boundary sub-parallel to the maximum compressive stress (Daines & Kohlstedt 1997; Zimmerman *et al.* 1999; Takei 2010). In addition, in shear experiments, melt-rich bands form at small strain rates, sub-parallel to the shear plane (Holtzman *et al.* 2003*a*, *b*; Takei & Holtzman 2009). Our results showed that low aspect ratio vertically aligned melt is present beneath the MER and the Red Sea Rift. Interestingly, the aspect ratios for vertically aligned melt beneath the MER are lower (0.02–0.2) than that for the Red Sea Rift (>0.1). Independent estimates of the amounts of melt beneath

Table 7. *Range of models that can explain seismic observations beneath Afar (Danakil microplate), but not including constraints on radial anisotropy*

Afar (Danakil microplate) (13° N, 41.5° E)	Melt fraction	Aspect ratio (vertical)	Aspect ratio (horizontal)
Disc-shaped vertical inclusions and any shaped horizontal inclusions	0.01–0.05	0.08–1.0	0.01–0.1
Tubular-shaped vertical inclusions and any shaped horizontal inclusions	0.01–0.05	1–100	0.01–0.1
Disc-shaped horizontal inclusions and any shaped vertical inclusions	0.01–0.05	0.08–100	0.01–0.1
Tubular-shaped horizontal inclusions and any shaped vertical inclusions			
Disc-shaped vertical inclusions and disc-shaped horizontal inclusions	0.01–0.05	0.08–1	0.01–0.1
Tubular-shaped vertical inclusions and tubular-shaped horizontal inclusions			
Vertical inclusions only (any aspect ratio)			
Horizontal inclusions only (any aspect ratio)	0.01–0.06		0.013–0.2

the DMH rift segment come from magnetotelluric studies (Desissa *et al.* 2013). These models of conductivity structure estimate that up to 13% melt is present in the uppermost mantle. In our models, this suggests that melt is stored in high aspect ratio (>1) tubular-like inclusions.

Our results support the idea of lateral variations in melt storage beneath Ethiopia. In the narrow MER and, to a lesser degree, the DMH rift segment, where seismic evidence shows very steep gradients in the lithosphere–asthenosphere topography (Rychert *et al.* 2012), mantle flow can cause large strain rates at the rift margins, resulting in significant shear-derived segregation of melt. This generates subvertical alignment of the melt bands. Beneath the DM, melt (1–6%) is stored in horizontally aligned low aspect ratio (0.013 − 0.2) structures. In this region, little topography is inferred on the lithosphere–asthenosphere boundary (Rychert *et al.* 2012), thus any shear due to mantle flow will act to align the melt in horizontal sheets.

Conclusions

It is evident that seismology provides limited constraints on the amount of melt, but can estimate the location, the orientation of any alignment and the probable shape of any melt present. This is particularly true when using multiple seismic attributes, showing that joint inversions for anisotropy in multiple seismic phases are needed (e.g. Brisbourne *et al.* 1999; Obrebski *et al.* 2010). Future studies incorporating other geophysical (e.g. magnetotelluric), geodetic (e.g. global positioning system or interferometric synthetic aperture radar) and geological (experimental petrology) techniques to try and place constraints on the amount of melt in the crust and mantle will assist seismic constraints on the geometry of melt. We cannot distinguish between the different mechanisms of melt segregation (e.g. dykes and sills, melt on grain boundaries, shear-derived segregation of melt) with the modelling approach used here as any alignment of melt on length scales smaller than the seismic wavelength will cause similar anisotropy. Studies investigating frequency dependence in anisotropy measurements in hydrocarbon reservoirs have shown that the size of fractures can be identified (Maultzsch *et al.* 2003; Al-Harrasi *et al.* 2011). Applying this to earthquake data to understand the size of melt inclusions has the potential to place more constraints on the mechanism of melt segregation in the crust and mantle.

We have shown how the presence of partial melt in the crust and mantle affects a variety of different seismic waves. This is summarized in Table 1, which provides a guide to future seismic studies aiming to identify melt from the analysis of seismic waves. We applied this improved understanding to place constraints on the nature of the partial melt present beneath the MER and Afar Depression, Ethiopia. We showed that low aspect ratio melts stored in vertical inclusions are present beneath the MER and Red Sea Rift, with larger melt fractions beneath the Red Sea Rift than the MER, whereas low aspect ratio melt in horizontal inclusions was found beneath the DM. This supports the idea of the shear-derived segregation of melt being a major component for the transport of melt from its place of generation to shallow depths.

We would like to thank the organizers of the Magmatic Rifting and Active Volcanism Conference 2012, Addis Ababa, Ethiopia for allowing us to attend and present at the conference, where initial discussions around this work occurred. Anna Stork is thanked for providing the Pn tomographic models. Stewart Fishwick is thanked for providing the surface wave tomographic models. Derek Keir and one anonymous reviewer are thanked for their comments on the manuscript. This work was supported by NERC grant NE/E007414/1. JOSH was supported by NERC Fellowship NE/1020342/1.

References

Al-Harrasi, O. H., Kendall, J.-M. & Chapman, M. 2011. Fracture characterization using frequency-dependent shear wave anisotropy analysis of microseismic data. *Geophysical Journal International*, **185**, 1059–1070, http://doi.org/10.1111/j.1365-246X.2011.04997.x

Annen, C., Blundy, J. D. & Sparks, R. S. J. 2006. The genesis of intermediate and silicic magmas in deep crustal hot zones. *Journal of Petrology*, **47**, 505–539, http://doi.org/10.1093/petrology/egi084

Armitage, J. J., Ferguson, D. J., Goes, S., Hammond, J. O. S., Calais, E., Rychert, C. A. & Harmon, N. 2015. Upper mantle temperature and the onset of extension and break-up in Afar, Africa. *Earth and Planetary Science Letters*, **418**, 78–90, http://doi.org/10.1016/j.epsl.2015.02.039

Ayele, A., Stuart, G. & Kendall, J. 2004. Insights into rifting from shear wave splitting and receiver functions: an example from Ethiopia. *Geophysical Journal International*, **157**, 354–362, http://doi.org/10.1111/j.1365-246X.2004.02206.x

Bastow, I. D., Stuart, G. W., Kendall, J. & Ebinger, C. J. 2005. Upper-mantle seismic structure in a region of incipient continental breakup: northern Ethiopian rift. *Geophysical Journal International*, **162**, 479–493, http://doi.org/10.1111/j.1365-246X.2005.02666.x

Bastow, I. D., Nyblade, A. A., Stuart, G. W., Rooney, T. O. & Benoit, M. H. 2008. Upper mantle seismic structure beneath the Ethiopian hot spot: rifting at the edge of the African low-velocity anomaly. *Geochemistry, Geophysics, Geosystems*, **9**, Q12022, http://doi.org/10.1029/2008GC002107

Bastow, I., Pilidou, S., Kendall, J. & Stuart, G. 2010. Melt-induced seismic anisotropy and magma assisted

rifting in Ethiopia: evidence from surface waves. *Geochemistry, Geophysics, Geosystems*, **11**, Q0AB05, http://doi.org/10.1029/2010GC003036

Belachew, M., Ebinger, C. J., Cote, D., Keir, D., Rowland, J., Hammond, J. O. S. & Ayele, A. 2011. Comparison of dike intrusions in an incipient seafloor spreading segment in Afar, Ethiopia: seismicity perspectives. *Journal of Geophysical Research*, **116**, B06405, http://doi.org/10.1029/2010JB007908

Benoit, M. H., Nyblade, A. A. & VanDecar, J. C. 2006. Upper mantle P-wave speed variations beneath Ethiopia and the origin of the Afar hotspot. *Geology*, **34**, 329–332, http://doi.org/10.1130/G22281.1

Blackman, D. K. & Kendall, J. 1997. Sensitivity of teleseismic body waves to mineral texture and melt in the mantle beneath a mid-ocean ridge. *Philosophical Transactions of the Royal Society of London Series A*, **355**, 217–231, http://doi.org/10.1098/rsta.1997.0007

Booth, D. C. & Crampin, S. 1985. Shear-wave polarizations on a curved wavefront at an isotropic free surface. *Geophysical Journal International*, **83**, 31–45, http://doi.org/10.1111/j.1365-246X.1985.tb05154.x

Brisbourne, A., Stuart, G. & Kendall, J. 1999. Anisotropic structure of the Hikurangi subduction zone, New Zealand – integrated interpretation of surface-wave and body-wave observations. *Geophysical Journal International*, **137**, 214–230, http://doi.org/10.1046/j.1365-246x.1999.00786.x

Buehler, J. S. & Shearer, P. M. 2014. Anisotropy and Vp/Vs in the uppermost mantle beneath the western United States from joint analysis of Pn and Sn phases. *Journal of Geophysical Research*, **119**, 1200–1219, http://doi.org/10.1002/2013JB010559

Chapman, M. 2003. Frequency-dependent anisotropy due to meso-scale fractures in the presence of equant porosity. *Geophysical Prospecting*, **51**, 369–379, http://doi.org/10.1046/j.1365-2478.2003.00384.x

Corbeau, J., Rolandone, F. *et al.* 2014. Uppermost mantle velocity from Pn tomography in the Gulf of Aden. *Geosphere*, **10**, 958–968, http://doi.org/10.1130/GES01052.1

Cornwell, D. G., Maguire, P. K. H., England, R. W. & Stuart, G. W. 2010. Imaging detailed crustal structure and magmatic intrusion across the Ethiopian rift using a dense linear broadband array. *Geochemistry, Geophysics, Geosystems*, **11**, Q0AB03, http://doi.org/10.1029/2009GC002637

Daines, M. & Kohlstedt, D. 1997. Influence of deformation on melt topology in peridotites. *Journal of Geophysical Research: Solid Earth (1978–2012)*, **102**, 10 257–10 271, http://doi.org/10.1029/97JB00393

Daly, E., Keir, D., Ebinger, C. J., Stuart, G. W., Bastow, I. D. & Ayele, A. 2008. Crustal tomographic imaging of a transitional continental rift: the Ethiopian rift. *Geophysical Journal International*, **172**, 1033–1048, http://doi.org/10.1111/j.1365-246X.2007.03682.x

Desissa, M., Johnson, N. E., Whaler, K. A., Hautot, S., Fisseha, S. & Dawes, G. 2013. A mantle magma reservoir beneath an incipient mid-ocean ridge in Afar, Ethiopia. *Nature Geosciences*, **6**, 861–865, http://doi.org/10.1038/ngeo1925

Dugda, M. T., Nyblade, A. A., Julia, J., Langston, C. A., Ammon, C. J. & Simiyu, S. 2005. Crustal structure in Ethiopia and Kenya from receiver function analysis: implications for rift development in eastern Africa. *Journal of Geophysical Research*, **110**, B01303, http://doi.org/10.1029/2004JB003065

Eshelby, J. D. 1957. The determination of the elastic field of an ellipsoidal inclusion, and related problem. *Proceedings of the Royal Society of London. Series A, Mathematical and Physical Sciences*, **241**, 376–396, http://doi.org/10.1098/rspa.1957.0133

Faul, U. H., Toomey, D. R. & Waff, H. S. 1994. Intergranular basaltic melt is distributed in thin, elongated inclusions. *Geophysical Research Letters*, **21**, 29–32, http://doi.org/10.1029/93GL03051

Ferguson, D., Maclennan, J. *et al.* 2013. Melting during late-stage rifting in Afar is hot and deep. *Nature*, **499**, 70–73, http://doi.org/10.1038/nature12292

Fishwick, S. 2010. Surface wave tomography: imaging of the lithosphere–asthenosphere boundary beneath central and southern Africa. *Lithos*, **120**, 63–73, http://doi.org/10.1016/j.lithos.2010.05.011

Forsyth, D. W., Scheirer, D. *et al.* 1998. Imaging the deep seismic structure beneath a mid-ocean ridge: the MELT experiment. *Science*, **280**, 1215–1218, http://doi.org/10.1126/science.280.5367.1215

Gao, S., Liu, K. & Abdelsalam, M. 2010. Seismic anisotropy beneath the Afar Depression and adjacent areas: implications for mantle flow. *Journal of Geophysical Research*, **115**, B12330, http://doi.org/10.1029/2009JB007141

Garapic, G., Faul, U. & Brisson, E. 2013. High-resolution imaging of the melt distribution in partially molten upper mantle rocks: evidence for wetted two-grain boundaries. *Geochemistry, Geophysics, Geosystems*, **14**, 556–566, http://doi.org/10.1029/2012GC004547

Gashawbeza, E. M., Klemperer, S. L., Nyblade, A. A., Walker, K. T. & Keranen, K. M. 2004. Shear-wave splitting in Ethiopia: Precambrian mantle anisotropy locally modified by Neogene rifting. *Geophysical Research Letters*, **31**, L18602, http://doi.org/10.1029/2004GL020471

Goes, S. & van der Lee, S. 2002. Thermal structure of the North American uppermost mantle inferred from seismic tomography. *Journal of Geophysical Research*, **107**, 2050, http://doi.org/10.1029/2000JB000049

Goes, S., Armitage, J., Harmon, N., Smith, H. & Huismans, R. 2012. Low seismic velocities below mid-ocean ridges: attenuation v. melt retention. *Journal of Geophysical Research*, **117**, B12403, http://doi.org/10.1029/2012JB009637

Guidarelli, M., Stuart, G., Hammond, J. O. S., Kendall, J., Ayele, A. & Belachew, M. 2011. Surface wave tomography across Afar, Ethiopia: crustal structure at a rift triple-junction zone. *Geophysical Research Letters*, **38**, L24313, http://doi.org/10.1029/2011GL046840

Hammond, J. O. S. 2014. Constraining melt storage geometries beneath the Afar Depression, Ethiopia from teleseismic receiver functions: the anisotropic H-κ stacking technique. *Geochemistry, Geophysics, Geosystems*, **15**, 1316–1332, http://doi.org/10.1002/2013GC005186

Hammond, J. O. S., Kendall, J., Angus, D. & Wookey, J. 2010. Interpreting spatial variations in anisotropy:

insights into the Main Ethiopian Rift from SKS waveform modelling. *Geophysical Journal International*, **181**, 1701–1712, http://doi.org/10.1111/j.1365-246X.2010.04587.x

Hammond, J. O. S., Kendall, J., Stuart, G. W., Keir, D., Ebinger, C. J., Ayele, A. & Belachew, M. 2011. The nature of the crust beneath the Afar triple junction: evidence from receiver functions. *Geochemistry, Geophysics, Geosystems*, **12**, Q12004, http://doi.org/10.1029/2011GC003738

Hammond, J. O. S., Kendall, J.-M. *et al.* 2013. Mantle upwelling and initiation of rift segmentation beneath the Afar Depression. *Geology*, **41**, 635–638, http://doi.org/10.1130/G33925.1

Hammond, J. O. S., Kendall, J.-M., Wookey, J., Stuart, G. W., Keir, D. & Ayele, A. 2014. Differentiating flow, melt or fossil seismic anisotropy beneath Ethiopia. *Geochemistry, Geophysics, Geosystems*, **15**, 1878–1894, http://doi.org/10.1002/2013GC005185

Hammond, W. & Humphreys, E. 2000. Upper mantle seismic wave velocity: effects of realistic partial melt geometries. *Journal of Geophysical Research*, **105**, 10 975–10 986, http://doi.org/10.1029/2000JB900041

Hearn, T. M. 1996. Anisotropic Pn tomography in the western United States. *Journal of Geophysical Research*, **101**, 8403–8414, http://doi.org/10.1029/96JB00114

Hearn, T. M. & Ni, J. F. 1994. Pn velocities beneath continental collision zones: the Turkish–Iranian Plateau. *Geophysical Journal International*, **117**, 273–283, http://doi.org/10.1111/j.1365-246X.1994.tb03931.x

Hearn, T. M., Wang, S., Ni, J. F., Xu, Z., Yu, Y. & Zhang, X. 2004. Uppermost mantle velocities beneath China and surrounding regions. *Journal of Geophysical Research*, **109**, B11301, http://doi.org/10.1029/2003JB002874

Holness, M. B. 2005. Melt–solid dihedral angles of common minerals in natural rocks. *Journal of Petrology*, **47**, 791–800, http://doi.org/10.1093/petrology/egi094

Holtzman, B. K. & Kendall, J. 2010. Organized melt, seismic anisotropy and plate boundary lubrication. *Geochemistry, Geophysics, Geosystems*, **11**, Q0AB06, http://doi.org/10.1029/2010GC003296

Holtzman, B. K. & Kohlstedt, D. L. 2007. Stress-driven melt segregation and strain partitioning in partially molten rocks: effects of stress and strain. *Journal of Petrology*, **48**, 2379–2406, http://doi.org/10.1093/petrology/egm065

Holtzman, B., Groebner, N., Zimmerman, M., Ginsberg, S. & Kohlstedt, D. 2003*a*. Stress-driven melt segregation in partially molten rocks. *Geochemistry, Geophysics, Geosystems*, **4**, 8607, http://doi.org/10.1029/2001GC000258

Holtzman, B. K., Kohlstedt, D. L., Zimmerman, F. H. M. E., Hiraga, T. & Hustoft, J. 2003*b*. Melt segregation and strain partitioning: implications for seismic anisotropy and mantle flow. *Science*, **301**, 1227–1230, http://doi.org/10.1126/science.1087132

Jackson, I., Fitzgerald, J. D., Faul, U. H. & Tan, B. H. 2002. Grain-size-sensitive seismic wave attenuation in polycrystalline olivine. *Journal of Geophysical Research*, **107**(B12), 2360, http://doi.org/10.1029/2001JB001225

Jakobsen, M. & Chapman, M. 2009. Unified theory of global flow and squirt flow in cracked porous media. *Geophysics*, **74**, WA65–WA76, http://doi.org/10.1190/1.3078404

Jaxybulatov, K., Shapiro, N. M., Koulakov, I., Mordret, A., Landes, M. & Sens-Schonfelder, C. 2014. A large magmatic sill complex beneath the Toba caldera. *Science*, **346**, 617–619, http://doi.org/10.1126/science.1258582

Karato, S. & Jung, H. 1998. Water, partial melting and the origin of the seismic low velocity and high attenuation zone in the upper mantle. *Earth and Planetary Science Letters*, **157**, 193–207, http://doi.org/10.1016/S0012-821X(98)00034-X

Keir, D., Kendall, J., Ebinger, C. J. & Stuart, G. W. 2005. Variations in late syn-rift melt alignment inferred from shear-wave splitting in crustal earthquakes beneath the Ethiopian rift. *Geophysical Research Letters*, **32**, L23308, http://doi.org/10.1029/2005GL024150

Keir, D., Belachew, M. *et al.* 2011. Mapping the evolving strain field during continental breakup from crustal anisotropy in the Afar Depression. *Nature Communications*, **2**, article no. 285, http://doi.org/10.1038/ncomms1287

Kelemen, P. B., Hirth, G. & Shimizu, N. 1997. A review of melt migration processes in the adiabatically upwelling mantle beneath oceanic spreading ridges. *Philosophical Transactions of the Royal Society of London Series A*, **355**, 283–318, http://doi.org/10.1098/rsta.1997.0010

Kendall, J. 1994. Teleseismic arrivals at a mid-ocean ridge: effects of mantle melt and anisotropy. *Geophysical Research Letters*, **21**, 301–304, http://doi.org/10.1029/93GL02791

Kendall, J., Stuart, G. W., Ebinger, C. J., Bastow, I. D. & Keir, D. 2005. Magma-assisted rifting in Ethiopia. *Nature*, **433**, 146–148, http://doi.org/10.1038/nature03161

Keranen, K. M., Klemperer, S. L., Julia, J., Lawrence, J. F. & Nyblade, A. A. 2009. Low lower crustal velocity across Ethiopia: is the Main Ethiopian Rift a narrow rift in a hot craton? *Geochemistry, Geophysics, Geosystems*, **10**, Q0AB01, http://doi.org/10.1029/2008GC002293

Mackenzie, G. D., Thybo, H. & Maguire, P. K. H. 2005. Crustal velocity structure across the Main Ethiopian Rift: results from two-dimensional wide-angle seismic modelling. *Geophysical Journal International*, **162**, 994–1006, http://doi.org/10.1111/j.1365-246X.2005.02710.x

Maguire, P. K. H., Ebinger, C. J. *et al.* 2003. Geophysical project in Ethiopia studies continental breakup. *EOS*, **84**, 337, http://doi.org/10.1029/2003EO350002

Maguire, P. K. H., Keller, G. R. *et al.* 2006. Crustal structure of the northern Main Ethiopian Rift from the EAGLE controlled-source survey: a snapshot of incipient lithospheric break-up. *In*: Yirgu, G., Ebinger, C. J. & Maguire, P. K. H. (eds) *The Afar Volcanic Province within the East African Rift System.* Geological Society, London, Special Publications, **259**, 269–292, http://doi.org/10.1144/GSL.SP.2006.259.01.21

MAKRIS, J. & GINZBURG, A. 1987. The Afar Depression: transition between continental rifting and sea-floor spreading. *Tectonophysics*, **141**, 199–214, http://doi.org/10.1016/0040-1951(87)90186-7

MAULTZSCH, S., CHAPMAN, M., LIU, E. & LI, X. Y. 2003. Modelling frequency-dependent seismic anisotropy in fluid-saturated rock with aligned fractures: implication of fracture size estimation from anisotropic measurements. *Geophysical Prospecting*, **51**, 381–392, http://doi.org/10.1046/j.1365-2478.2003.00386.x

MINARIK, W. G. & WATSON, E. B. 1995. Interconnectivity of carbonate melt at low melt fraction. *Earth and Planetary Science Letters*, **133**, 423–437, http://doi.org/10.1016/0012-821X(95)00085-Q

NYBLADE, A. A. & LANGSTON, C. A. 2002. Broadband seismic experiments probe the East African Rift. *EOS*, **83**, 407–408, http://doi.org/10.1029/2002EO000296

OBREBSKI, M., KISELEV, S., VINNIK, L. & MONTAGNER, J. 2010. Anisotropic stratification beneath Africa from joint inversion of SKS and P receiver functions. *Journal of Geophysical Research*, **115**, B09313, http://doi.org/10.1029/2009JB006923

PEI, S., ZHAO, J. *ET AL.* 2007. Upper mantle seismic velocities and anisotropy in China determined through Pn and Sn tomography. *Journal of Geophysical Research*, **112**, B05312, http://doi.org/10.1029/2006JB004409

POMMIER, A. & GARNERO, E. J. 2014. Petrology based modeling of mantle melt electrical conductivity and joint interpretation of electromagnetic and seismic results. *Journal of Geophysical Research*, **119**, 4001– 4016, http://doi.org/10.1002/2013JB010449

POMMIER, A., LEINENWEBER, K., KOHLSTEDT, D. L., QI, C., GARNERO, E. J., MACKWELL, S. J. & TYBURCZY, J. A. 2015. Experimental constraints on the electrical anisotropy of the lithosphere–asthenosphere system. *Nature*, **522**, 202–206, http://doi.org/10.1038/nature14502

ROONEY, T., FURMAN, T., YIRGU, G. & AYALEW, D. 2005. Structure of the Ethiopian lithosphere: xenolith evidence in the Main Ethiopian Rift. *Geochimica Cosmochimica Acta*, **69**, 3889–3910, http://doi.org/10.1016/j.gca.2005.03.043

RYCHERT, C. A., HAMMOND, J. O. S. *ET AL.* 2012. Volcanism in the Afar rift sustained by decompression melting with minimal plume influence. *Nature Geoscience*, **5**, 406–409, http://doi.org/10.1038/NGEO1455

SCHMELING, H. 1985. Numerical models on the influence of partial melt on elastic, anelastic and electric properties of rocks. Part I: elasticity and anelasticity. *Physics of the Earth and Planetary Interiors*, **41**, 34–57, http://doi.org/10.1016/0031-9201(85)90100-1

SEBAI, A., STUTZMANN, E., MONTAGNER, J., SICILIA, D. & BEUCLER, E. 2006. Anisotropic structure of the African upper mantle from Rayleigh and Love wave tomography. *Physics of the Earth and Planetary Interiors*, **155**, 48–62, http://doi.org/10.1016/j.pepi.2005.09.009

SICILIA, D., MONTAGNER, J. *ET AL.* 2008. Upper mantle structure of shear-waves velocities and stratification of anisotropy in the Afar hotspot region. *Tectonophysics*, **462**, 164–177, http://doi.org/10.1016/j.tecto.2008.02.016

STIXRUDE, L. & LITHGOW-BERTELLONI, C. 2005. Mineralogy and elasticity of the oceanic upper mantle: origin of the low-velocity zone. *Journal of Geophysical Research*, **110**, B03204, http://doi.org/10.1029/2004JB002965

STORK, A., STUART, G. W., HENDERSON, C. M., KEIR, D. & HAMMOND, J. O. S. 2013. Uppermost mantle (Pn) velocity model for the Afar region, Ethiopia: an insight into rifting processes. *Geophysical Journal International*, **193**, 321–328, http://doi.org/10.1093/gji/ggs106

STUART, G. W., BASTOW, I. D. & EBINGER, C. J. 2006. Crustal structure of the northern Main Ethiopian Rift from receiver function studies. *In*: YIRGU, G., EBINGER, C. J. & MAGUIRE, P. K. H. (eds) *The Afar Volcanic Province within the East African Rift System*. Geological Society, London, Special Publications, **259**, 253–267, http://doi.org/10.1144/GSL.SP.2006. 259.01.20

TAKEI, Y. 2010. Stress-induced anisotropy of partially molten rock analogue deformed under quasi-static loading test. *Journal of Geophysical Research*, **115**, B03204, http://doi.org/10.1029/2009JB006568

TAKEI, Y. 2013. Elasticity, anelasticity, and viscosity of a partially molten rock. *In*: KARATO, S. (ed.) *Physics and Chemistry of the Deep Earth*. Wiley-Blackwell, Oxford, 66–93.

TAKEI, Y. & HOLTZMAN, B. K. 2009. Viscous constitutive relations of solid–liquid composites in terms of grain boundary contiguity: 3. Causes and consequences of viscous anisotropy. *Journal of Geophysical Research*, **114**, B06206, http://doi.org/10.1029/2008JB005852

TANDON, G. P. & WENG, G. J. 1984. The effect of aspect ratio of inclusions on the elastic properties of unidirectionally aligned composites. *Polymer Composites*, **5**, 327–333, http://doi.org/10.1002/pc.750050413

WALKER, A. M. & WOOKEY, J. 2012. MSAT – a new toolkit for the analysis of elastic and seismic anisotropy. *Computers and Geosciences*, **49**, 81–90, http://doi.org/10.1016/j.cageo.2012.05.031

WANG, Y., FORSYTH, D. W. & SAVAGE, B. 2009. Convective upwelling in the mantle beneath the Gulf of California. *Nature*, **462**, 499–501, http://doi.org/10.1038/nature08552

WEST, M., MENKE, W., TOLSTOY, M., WEBB, S. & SOHN, R. 2001. Magma storage beneath axial volcano on the Juan de Fuca mid-ocean ridge. *Nature*, **413**, 833–836, http://doi.org/10.1038/35101581

WIRTH, E. & LONG, M. D. 2010. Frequency-dependent shear wave splitting beneath the Japan and Izu-Bonin subduction zones. *Physics of the Earth and Planetary Interiors*, **181**, 141–154, http://doi.org/10.1016/j.pepi.2010.05.006

XU, L., RONDENAY, S. & VAN DER HILST, R. D. 2007. Structure of the crust beneath the southeastern Tibetan plateau from teleseismic receiver functions. *Physics of the Earth and Planetary Interiors*, **165**, 176–193, http://doi.org/10.1016/j.pepi.2007.09.002

ZIMMERMAN, M. E., ZHANG, S., KOHLSTEDT, D. L. & KARATO, S. 1999. Melt distribution in mantle rocks deformed in shear. *Geophysical Research Letters*, **26**, 1505–1508, http://doi.org/10.1029/1999GL900259